Vol. 9, No. 2, April 2025, pp. 130-140

Current Optics and Photonics

Regular Paper

Design and Fabrication of Micro-binary Diffractive Optical Elements to Generate Airy Beams Using a Versatile Direct Laser Lithography Machine

Hieu Tran Doan Trung[1,2], Young-Sik Ghim[1,2]*, and Hyug-Gyo Rhee[1,2]**

[1]*Department of Science of Measurement, University of Science and Technology, Daejeon 34113, Korea*
[2]*Length and Dimensional Metrology Group, Physical Metrology Division, Korea Research Institute of Standards and Science, Daejeon 34113, Korea*

(Received January 22, 2025 : revised March 4, 2025 : accepted March 14, 2025)

Airy beam applications such as optical trapping, micro-machining, and imaging microscopy have garnered significant attention in recent years. This research introduces a comprehensive methodology for the design, simulation, fabrication, and evaluation of micro-binary diffractive optical elements aimed at generating Airy beams. First, a binary pattern is meticulously designed by means of computer-generated holography. Subsequently, the optical performance of the pattern is simulated using a Fresnel impulse response propagator, which is rooted in the Rayleigh–Sommerfeld diffraction in Fourier optics. Following this, a laser writing path is generated through a machine learning decision tree algorithm. A multifunctional direct laser lithography system is then used to fabricate the pattern. Lastly, a meticulous assessment of the surface quality is conducted, and an optical verification system is established to confirm the optical performance. This holistic process is characterized by its simplicity, self-contained nature, and cost-effectiveness due to its independence from masks, unlike traditional methods such as photolithography, ensuring a high level of accuracy. Moreover, it is important to note that this process is not only suitable for fabricating Airy beam diffractive optical elements, but also has the potential to generate other binary diffractive optical elements, notably on the micro-scale.

Keywords : Airy beam, Computer generated hologram, Diffractive optics, Direct laser lithography, Fourier optics
OCIS codes : (050.1970) Diffractive optics; (070.0070) Fourier optics and signal processing; (140.0140) Lasers and laser optics; (220.3740) Lithography

I. INTRODUCTION

Diffractive optical elements (DOEs) were invented to deflect light into different orders and angles, and they have two noticeable advantages. On the one hand, DOEs can work at special wavelengths, for instance ultra violet (UV) light [1], X-rays [2, 3], or gamma rays [4]. On the other hand, DOEs can form unique focal spots such as a vortex beam [5, 6] for transdermal drug delivery [7] and X-ray microscopy [8] or a Bessel beam [9, 10] to cut glass [11] and for light sheet microscopy [12]. As a result, DOEs are currently attracting more and more attention. Additionally, an Airy beam (AB) is one in which optical waves move along a curved trajectory [13–15]. ABs are well known due to their use in optical trapping [16, 17], micro-machining [18, 19], and microscopy [20, 21]. Specifically, ABs can be generated by binary DOEs, even on the micro-scale, and thus offer a complete process to design, simulate, fabricate,

*Corresponding author: young.ghim@kriss.re.kr, ORCID 0000-0002-4052-4939
**Corresponding author: hrhee@kriss.re.kr, ORCID 0000-0003-3614-5909

Color versions of one or more of the figures in this paper are available online.

pISSN: 2508-7266 / eISSN: 2508-7274 https://doi.org/10.3807/COPP.2025.9.2.130

and evaluate DOE patterns to generate ABs. In this study, we present a comprehensive approach for the fabrication of an amplitude AB DOE that independently generates an Airy beam without the requirement for lenses or additional support equipment. Our method is notably straightforward, efficient, reliable, and cost-effective, and facilitates the production of various binary DOEs in a wide range of complex geometries.

Firstly, computer-generated holography (CGH) [22, 23] is employed to create an axicon Fresnel zone plate DOE pattern, which generates a conical wave and a beam path steering element (BPSE). These elements are combined to form a new DOE capable of producing an AB. A Fresnel impulse response propagator, based on Rayleigh–Sommerfeld diffraction in Fourier optics, is used to predict the focal spot of the DOE. Following this, a decision tree algorithm in machine learning is employed to generate the laser writing path from the binary matrix of the DOE pattern. The design simulation and laser generation steps are facilitated with MATLAB Simulink R2020b. Subsequently, the laser writing path coordinates are transferred to a direct laser lithography (DLL) system.

DLL is renowned for having several advantages, such as not requiring a mask to create a high-resolution DOE pattern, good cost-effectiveness, and operability in general room conditions. The effectiveness of DLL has been demonstrated in previous research on binary DOE manufacturing [24–27], even on cylindrical surfaces [28]. In some instances, AB DOE patterns have been manufactured using a digital micro-mirror device (DMD) [29] or by means of electron-beam direct writing (EDW) [30]. While a DMD provides a quick solution to create a DOE pattern, EDW can fabricate detailed DOE patterns without requiring a mask. However, both methods have drawbacks that must be considered. For instance, DMD or a spatial light modulator can require many supporting optical elements that increase the complexity of the optics system, while EDW will incur a high cost and requires a complicated setup and a long fabrication time. Consequently, the DLL method is presented as an alternative alongside DMD, EDW, or any other method due to its advantages. In the final stage, the AB DOE pattern is validated for its surface quality and optical performance capabilities. It is important to note that the AB DOE pattern can generate the AB by itself without any supporting optical elements. The entire process is illustrated in Fig. 1(a).

This paper is structured as follows: Section II details the design and simulation method of the AB DOE pattern, Section III describes the fabrication method and presents the experiment and results, and Section IV provides the conclusion of the paper.

II. DESIGN AND SIMULATION

2.1. Design Method

In the first stage, the AB DOE pattern must be carefully designed and simulated to define both its shape and its optical performance. The primary objective of this stage is to employ CGH to generate the AB DOE binary matrix, which serves as the input for the simulation and laser path generation step. Previous research [31] has demonstrated that the potential-free Schrödinger equation can be used as below:

$$j\frac{\partial \phi}{\partial \xi} + \frac{1}{2}\frac{\partial^2 \phi}{\partial s^2} = 0. \tag{1}$$

The Airy Accelerating equation [32, 33] is expressed here as Eq. (2):

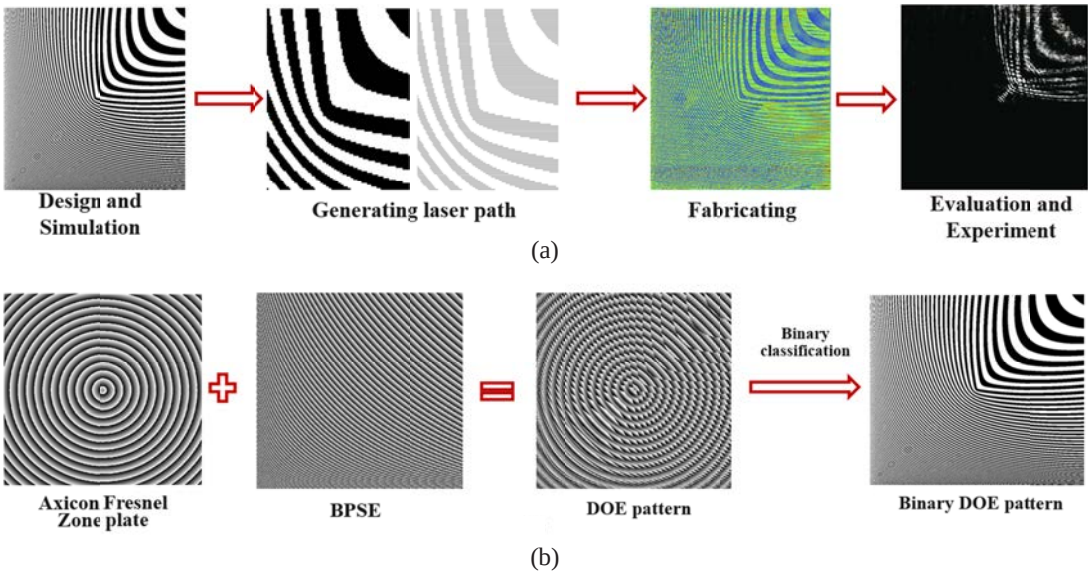

FIG. 1. Entire manufacturing process of (a) the Airy beam diffractive optical element (AB DOE) and (b) an AB DOE pattern design method by computer-generated holography (CGH).

$$\varnothing(\xi, s) = A\left(s - \left(\frac{\xi}{2}\right)^2\right)\exp\left(j\frac{s\xi}{2} - j\frac{\xi^3}{12}\right), \quad (2)$$

where $\varnothing$ is the electric field envelope, $s = x / x_0$ is a dimensionless transverse coordinate, x_0 is an arbitrary transverse scale, $\xi = z / kx_0^2$ is the normalized propagation distance and $k = 2\pi n / \lambda_0$. In addition, the trajectory is described by $(\xi / 2)^2$ and $A(s) = \varnothing(0, s)$ at the origin. Based on these equations, different methods of designing and generating a binary AB DOE pattern have been studied [29, 30]. In this research, a straightforward method is employed to compute the AB DOE pattern using CGH in the MATLAB Simulink R2020b software. The AB DOE pattern represents a combination of a conical wave generated by an axicon Fresnel zone plate [Eq. (3)] and a BPSE [Eq. (4)] [34] prior to entering the binary classification process [Fig. 1(b)]. The equation for the binary AB DOE pattern is expressed as

$$A = D\exp[2\pi j(\frac{r}{\lambda})\tan(\theta)], \quad (3)$$

$$B = E\exp\left[j\left(10\sqrt{\frac{y}{n} + \frac{M}{2}} + 10\sqrt{\frac{x}{n} + \frac{M}{2}}\right)\right], \quad (4)$$

where $r = \sqrt{x^2 + y^2}$, x and y are the coordinates, λ is the wavelength, θ is the angle to control the curvature, n is the resolution of the matrix or pixel pitch, M is the number of rows and columns of the matrix, and D and E are constants. Simply, the constants D and E control the thickness of the curves and the angle adjusts the curvature, while M and n determine the dimensions of the pattern. Depending on the design purpose, these parameters can be changed to control the shape of the DOE pattern. As a result, the AB DOE pattern is formed by combining A and B in a binary classification process. The transparent area is represented by 0-pixels and the opaque area is represented by 1-pixels.

2.2. Optical Simulation

In the following stage, a Fresnel impulse response propagator is used to simulate the optical performance of the AB DOE pattern, based on the theoretical Rayleigh–Sommerfeld diffraction solution I [35]:

$$U'(u,v) = \iint U(x,y)\, h(u - x, v - y)\, dxdy, \quad (5)$$

where the standard equation of the Rayleigh-Sommerfeld impulse response is:

$$h(u,v) = \frac{z}{j\lambda}\frac{\exp(jpq)}{r^2}, \quad (6)$$

and

$$q = \sqrt{z^2 + u^2 + v^2}. \quad (7)$$

$U'(u, v)$ is the propagation result of the $U(x, y)$ source plane, z is the propagation distance and $p = 2\pi / \lambda$. In certain instances, if there are adjustments to the distance propagation, focal length, or dimensions of the DOE, it may be necessary to investigate alternative propagation methods to maintain the accuracy of the simulation [36–38]. In Table 1, DOE patterns with varying parameters are presented to elucidate their influence on the shape and focal spot of the AB DOE patterns depicted in Fig. 2.

In this section, we present a methodology for the design and optical simulation of AB DOE patterns using CGH and the Fresnel impulse response propagator method. The process is implemented using MATLAB Simulink R2020b software. To validate the design and simulation process, we use the AB DOE pattern illustrated in Fig. 2(c) as a case study for subsequent fabrication and verification in the following sections. The resulting binary matrix of the AB DOE pattern serves as the basis for defining the laser path coordinates, and it is fabricated by means of DLL in the subsequent section.

III. FABRICATION AND EXPERIMENT

3.1. Fabrication Results

In the preceding section, we obtained a binary matrix that enables the direct generation of laser paths in MATLAB Simulink R2020b without the need for additional software. This approach provides precise control over all parameters, ensuring the efficiency of the system.

Initially, the position of each pixel in the binary matrix result is transformed into the coordinates of the DOE pattern. 0-pixels are designated as NaN (Not a Number), and the locations of 1-pixels in the row and column are marked to construct the coordinate matrix. Subsequently, the coordinate matrix is multiplied by the pixel pitch n from the previous section to convert the coordinates to real-life dimensions in the DLL machine. Finally, the machine learning decision tree algorithm is used to scan each row

TABLE 1. Airy beam diffractive optical element (AB DOE) parameters

M	n (um)	λ (nm)	θ (degree)	D	E	Propagation Distance (mm)
750	4	632.8	0.05	0.5	0.5	75
750	4	632.8	0.3	1	1	75
750	4	632.8	0.3	0.5	0.5	75

(or column), connect every point, and to skip NaN points to reduce the calculation capacity and manufacturing time. The laser path coordinates are input into the DLL system to manufacture the DOE pattern, as depicted in Fig. 3.

The entire process from Section II to the generation of all laser path coordinates in Section III was computed in 18 seconds using MATLAB Simulink R2020b on a laptop (Dell Latitude 7390, Intel Core i7-8650U CPU @ 1.90 GHz 2.11 GHz, 16 GB of RAM; Dell Technologies Inc., TX, USA).

The diagram presented in Fig. 4(a) details the operational process of the DLL system. First, (1) a laser source is activated to produce a laser beam. Following this, (2) an acousto-optic modulator is used to regulate the beam's intensity before it traverses through the (3) shutter. The shutter, with (4, 5, 6) three mirrors serves to obstruct the beam path as required, then redirects the laser beam to the (7) laser writing head. The (8) specimen is precisely fixed on (9, 10) linear stages X and Y. Notably, the entire system

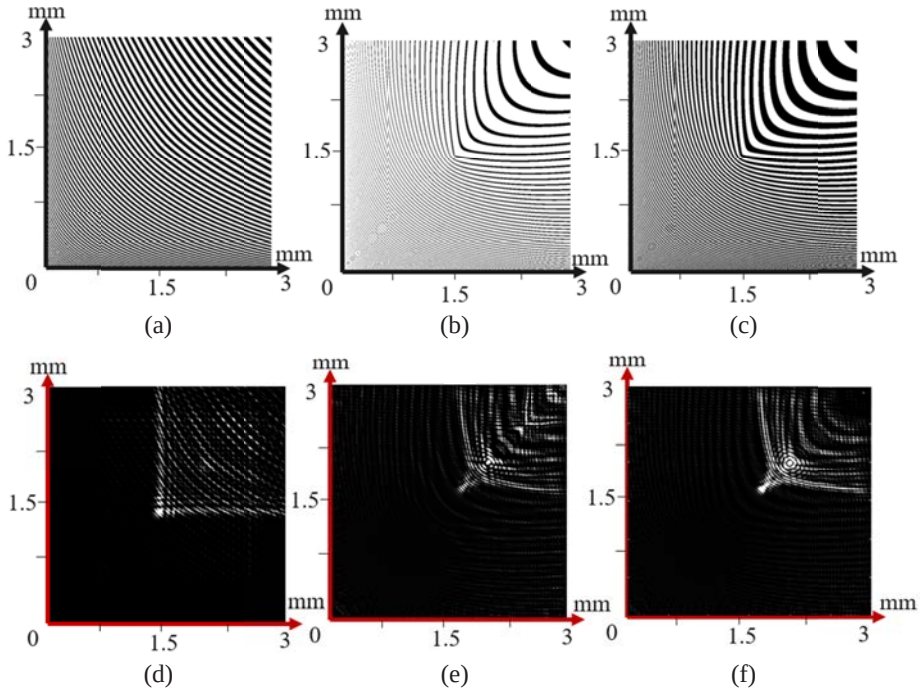

FIG. 2. Airy beam diffractive optical element (AB DOE) (a) with $D = E = 0.5$ and $\theta = 0.05$, (b) with $D = E = 1$ and $\theta = 0.3$, and (c) with $D = E = 0.5$ and $\theta = 0.3$, (d) simulation results of the DOE pattern in (a), (e) simulation results of the DOE pattern in (b), and (f) simulation results of the DOE pattern in (c). The *x*- and *y*-axis in (a) to (f) represent a pattern size in those directions.

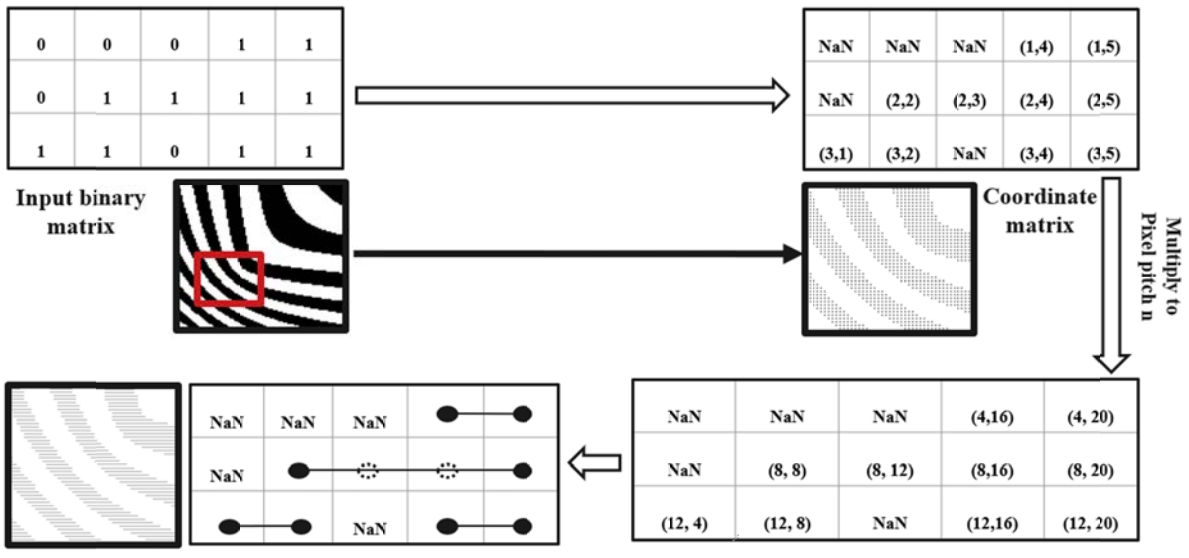

FIG. 3. Explanation of laser paths generated by the decision tree learning algorithm.

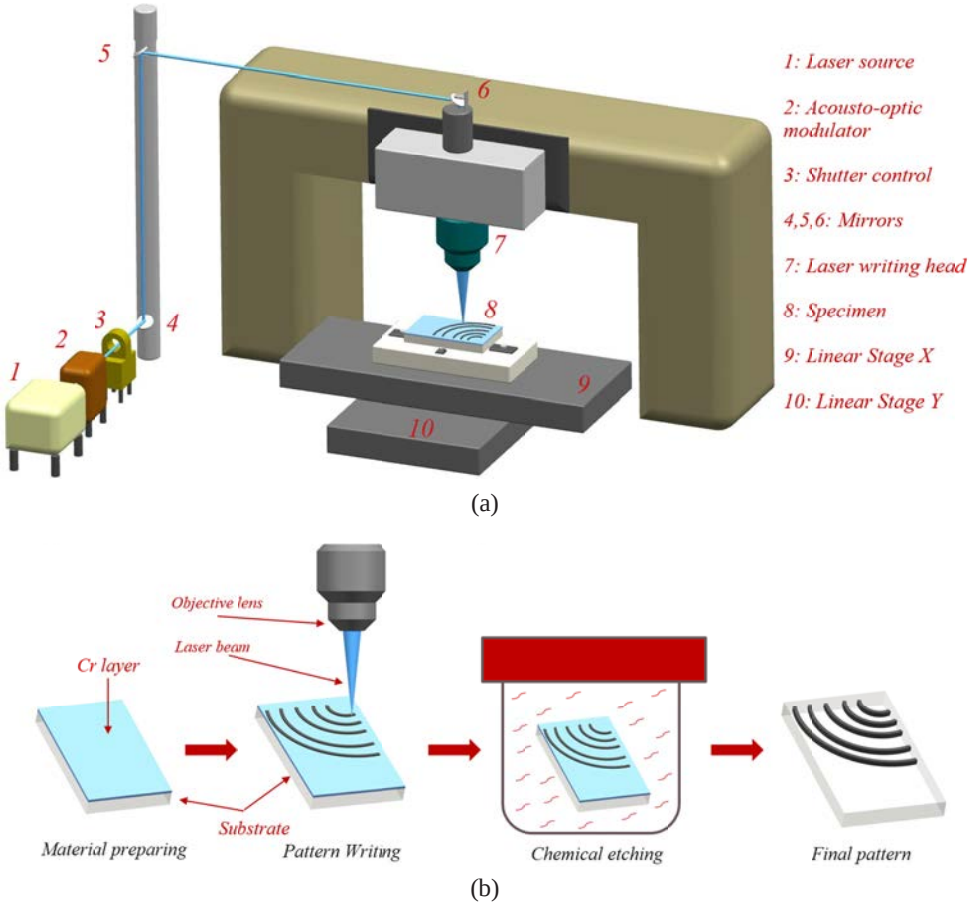

FIG. 4. Schematic diagram of (a) the direct laser lithography (DLL) system and (b) its fabrication process.

is intricately integrated with the control system for efficient and coordinated functionality.

The fabrication process of the DOE using the DLL system is visually presented in Fig. 4(b). It starts with the preparation of a glass substrate with a refractive index close to 1 and a chromium (Cr) layer (70 μm) on top its surface, and progresses with the importation of the laser paths from the previous stage into the DLL system for inscription of the desired pattern on the surface. Under the influence of the laser beam (514.5 nm), the Cr undergoes a conversion into chromium(III) oxide (Cr_2O_3). Subsequently, a five-minute etching procedure is conducted using a chemical solution consisting of $K_3[Fe(CN)_6]$ and NaOH to eliminate the Cr layer while safeguarding the Cr_2O_3 content. This meticulous sequence of steps culminates in the successful fabrication of the DOEs.

Figure 5(a) shows the results of the fabrication process after following the procedure outlined in Section II and Section III. Comparison between the simulation results and the fabrication results [Figs. 5(b) and 5(c)] indicates a good match. Further details regarding the surface measurement results and optical verification of the AB DOE pattern will be given in the following section.

3.2. Experiment and Results

This section provides a thorough analysis of the surface measurement findings and optical capabilities of each DOE. Surface measurements were carried out using a commercial nano surface profiler (NV-2400; Nano System Co. Ltd., Daejeon, Korea).

The AB DOE pattern is presented in Fig. 5(d), which provides a comprehensive global view. Moreover, local views are depicted in Figs. 6 and 7. Specifically, Figs. 5(d), 6(a), and 7(a) depict the overall shape of the DOE local view, showing a perfect match with the simulation results presented in Fig. 2(c). Furthermore, the 3D representations in Figs. 6(c) and 7(c), along with the surface measurements on the *x*- and *y*-axes, reveal stable surface profiles, indicative of flawless fabrication. These findings emphasize the robustness, efficiency, and precision of the design and fabrication process, which has consistent outcomes from conceptualization to production.

In order to assess the optical performance of the DOEs, a precise optical system was meticulously assembled [Fig. 8(a)]. This system consists of a (1) He-Ne laser as a beam source, with a specific wavelength of 632.8 nm. To adjust the intensity for the CMOS camera, a meticulous method was employed, involving the use of (2, 3) two lenses to expand the laser beam and a (4) filter. Notably, the experiment

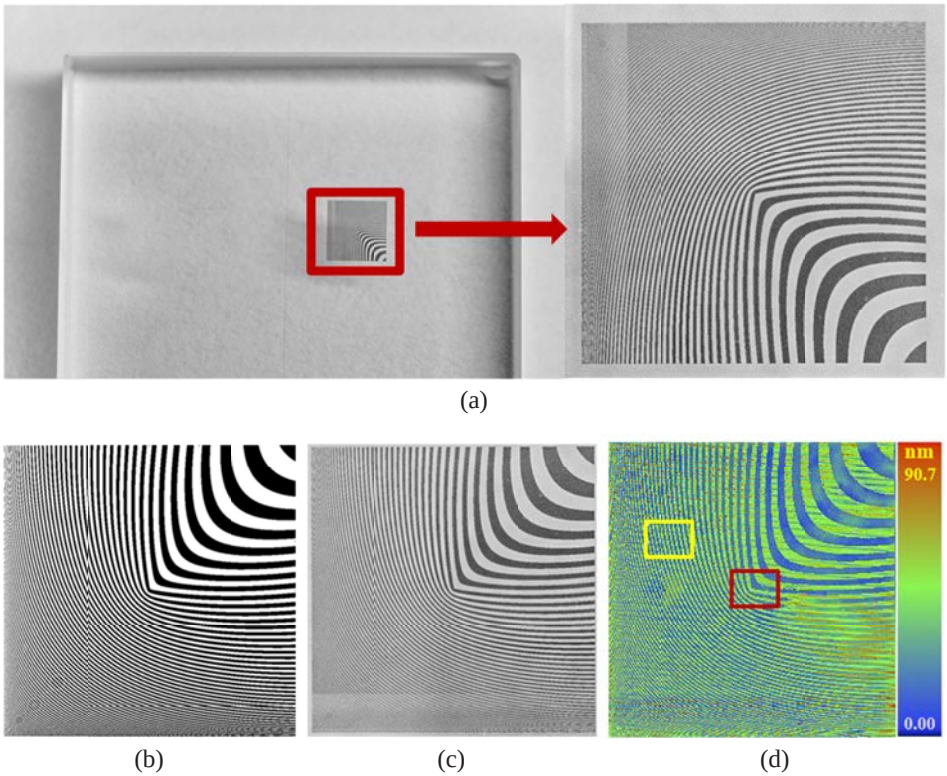

(a)

(b) (c) (d)

FIG. 5. Fabrication results: (a) Photographic view of the pattern, (b) the simulation and (c) the experimental results, (d) the 3D shape of the pattern obtained by a commercial white-light scanning interferometer.

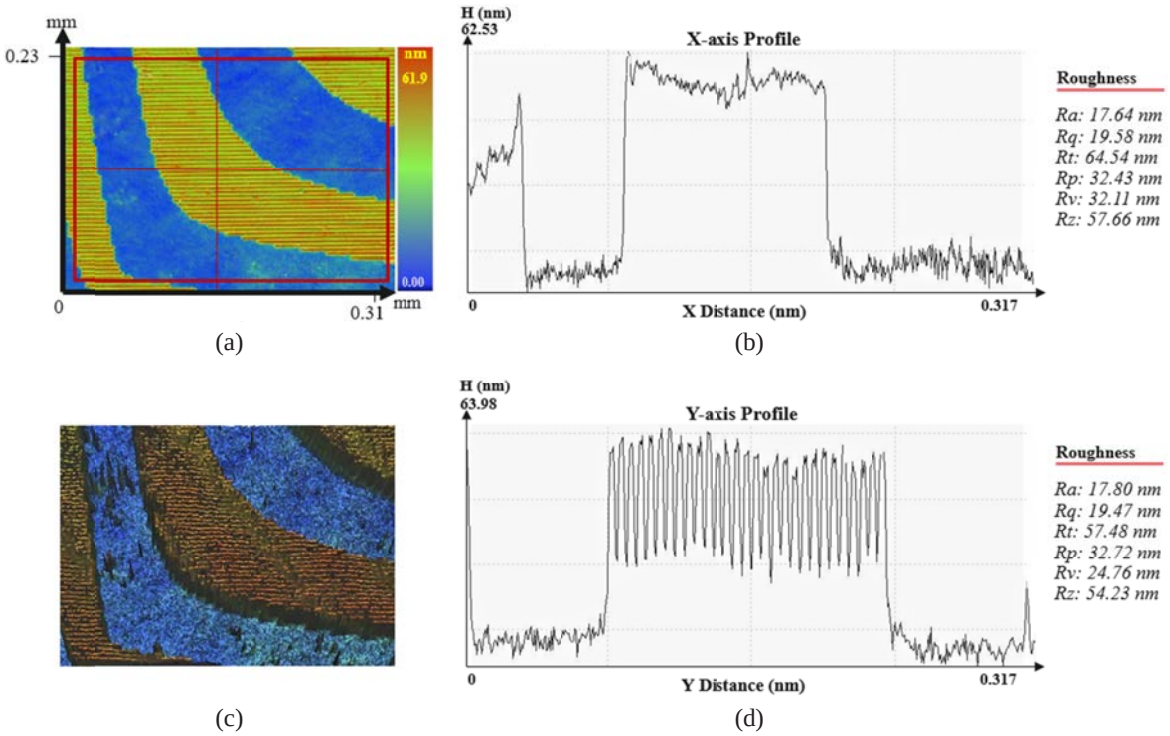

(a) (b)

(c) (d)

FIG. 6. Measurement results of (a) the Airy beam diffractive optical element (AB DOE) in Fig. 5(d) (red box), (b) its *x*-profile, (c) the 3D view, and (d) the *y*-profile.

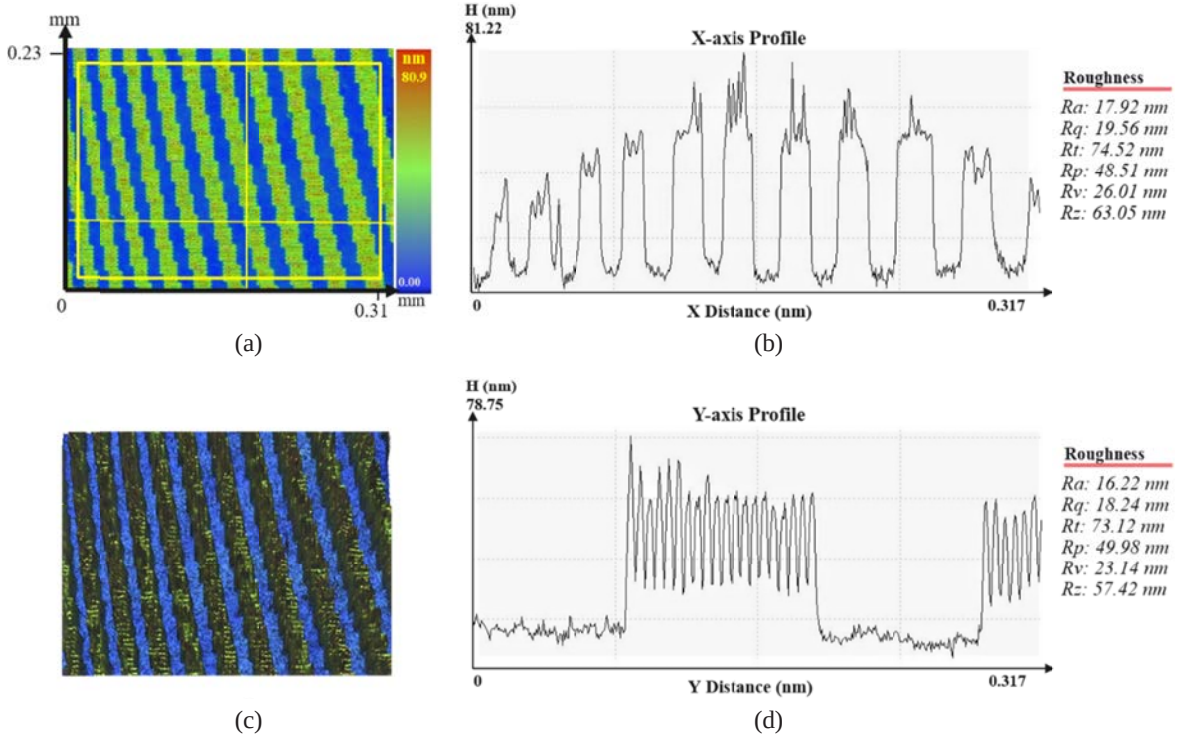

FIG. 7. Measurement results of (a) the Airy beam diffractive optical element (AB DOE) pattern in Fig. 5(d) (yellow box), (b) its *x*-profile, (c) the 3D view, and (d) the *y*-profile.

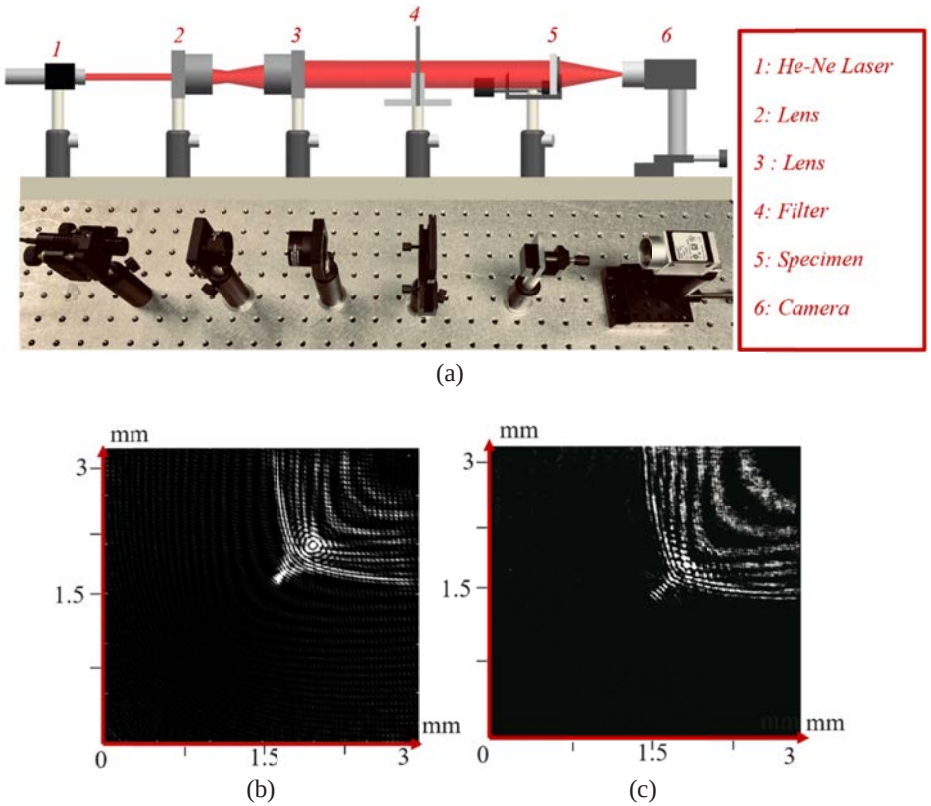

FIG. 8. Photographic view of (a) an optical evaluation system setup, (b) the simulation and (c) experiment images. The *x*- and *y*-axis in (b) and (c) represent a pattern size in those directions.

made use of a AC254-030-A-ML lens (with a focal length of 30 mm and diameter of 25.4 mm, BBARR COATING 400–700 nm, N-BAF10/N-SF6HT; Thorlabs Co., NJ, USA) and a AC254-300-A-ML lens (with a focal length of 300 mm and diameter of 25.4 mm, BBARR COATING 400–700 nm, N-BK7/SF2; Thorlabs Co.). The (5) specimen was accurately positioned in front of the (6) CMOS camera on a movable stage. It is essential to note that no additional equipment was used to augment the performance of the DOEs, thus ensuring that the experimental outcomes provide an accurate representation of the performance capabilities of the DOEs.

The experimental image presented in Fig. 8(c) exhibits a strong correlation with the simulated image in Fig. 8(b), indicating a high degree of consistency between the two. This alignment suggests that the design, simulation, and fabrication processes employed are not only reliable but also accurate, effectively validating the methodologies used throughout the study.

Furthermore, AB DOE can be further enhanced by integrating a Fresnel zone plate with the AB DOE (the Fresnel zone plate must have the same dimensions, resolution, and row-column number in comparison with the AB DOE), for instance an AB DOE that is similar to the AB DOE in Fig. 2(a). This innovative combination results in a new type of DOE capable of generating dual amplitude beams with improved focus without a lens or other support equipment. The enhancement is primarily attributed to the superior light-focusing characteristics of the Fresnel zone plate, which is recognized for its ability to concentrate light into a small focal point and is an effective alternative to traditional lenses in various applications.

The equation of the Fresnel zone plate is given below:

$$F = \exp\frac{(j\pi r^2)}{\lambda f}, \tag{8}$$

where $r = \sqrt{x^2 + y^2}$, x and y are the coordinates, λ is the wavelength, and f is the focal length equal to 40 mm. The construction of the new AB DOE is illustrated in Fig. 9(a), and its optical simulation is presented in Fig. 9(b). The manufacturing results of this new design are depicted in Fig. 9(c). The parameters employed in the fabrication of the new AB DOE are detailed in Table 2.

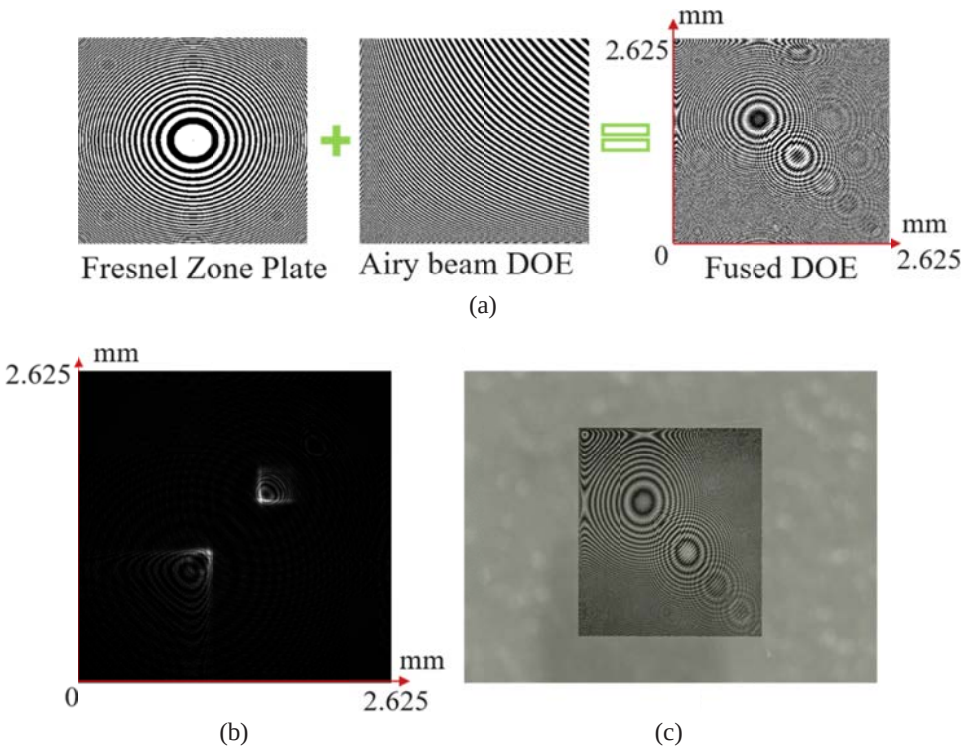

FIG. 9. A new Airy beam diffractive optical element (AB DOE) formation: (a) A typical design and its image obtained by (b) a simulation and (c) a fabrication. The *x*- and *y*-axis in (a) and (b) represent a pattern size in those directions.

TABLE 2. New Airy beam diffractive optical element (AB DOE) parameters

M	n (μm)	λ (nm)	θ (degree)	D	E	Propagation Distance (mm)
750	3.5	632.8	0.05	0.5	0.5	40

The evaluation of the new DOE is depicted in Figs. 10 and 11. It is evident that the geometric characteristics of the new DOE align closely with the simulation results. Additionally, there is a significant improvement in focus capability compared to the previous DOE design. Figure 11 provides a comparative analysis of the focus ability at vari-

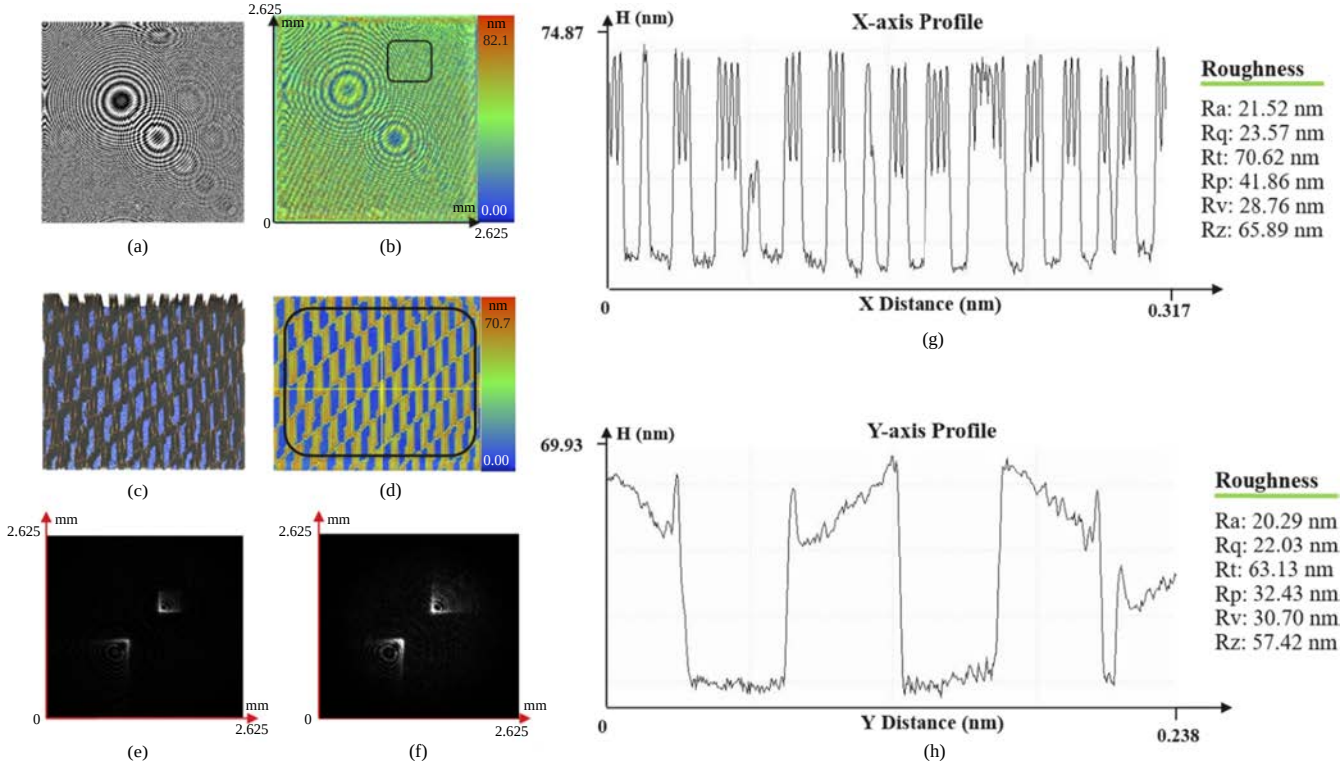

FIG. 10. Simulation and experimental results of the combined Airy beam diffractive optical element (AB DOE): (a) Simulation result, (b) its global view, (c) and (d) local view of the new AB DOE, (e) simulation image, (f) experiment image, (g) and (h) surface profile of (d).

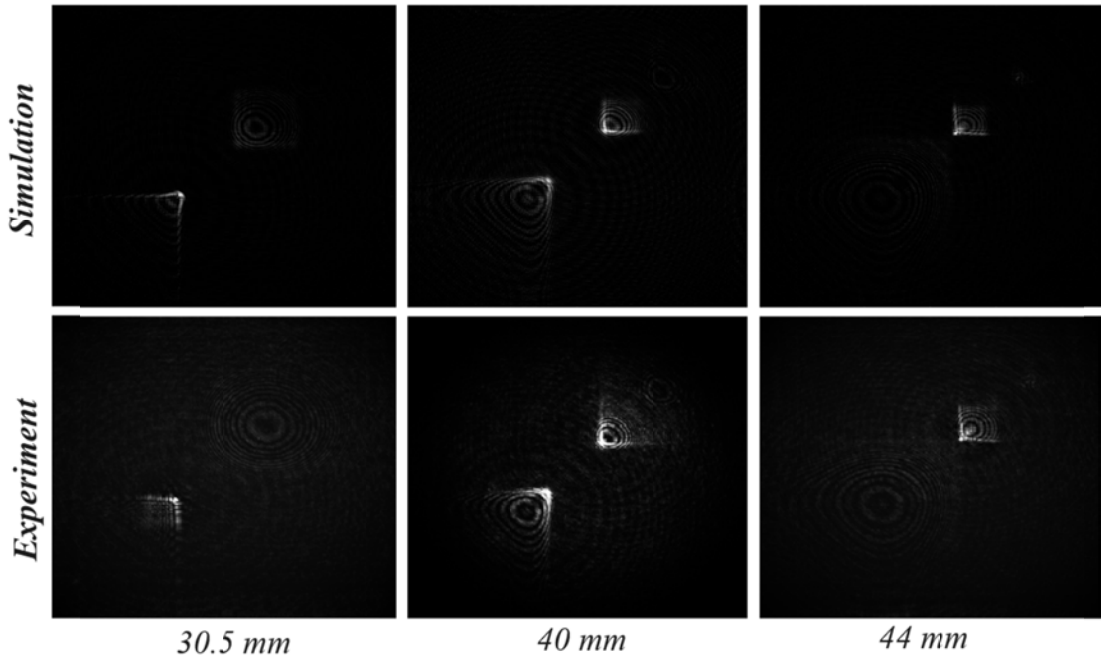

FIG. 11. Optical performance of new Airy beam diffractive optical element (AB DOE) in different positions in simulation and experiment.

ous positions, thereby substantiating the superior optical performance of the new AB DOE in terms of focal depth. The new AB DOE is generated on a dual beam at 40 mm while remaining only one beam at 30.5 and 44 mm. The focal length can be optimized by changing the parameters of AB DOE and focal length of the Fresnel zone plate.

The present section introduces a comprehensive procedure for assessing the surface quality and optical performance of AB DOE patterns after they are manufactured. The findings indicate exemplary surface quality and affirm the efficacy of the fabrication method. Additionally, the precision of the optical performance of AB DOE patterns, as evidenced in comparison to the simulation process, underscores the suitability of the design and simulation for the calculation of AB DOE patterns. The applicability of this comprehensive methodology surpasses AB DOE. patterns and encompasses a range of other binary DOE patterns, thereby establishing its suitability for broad-spectrum manufacturing.

IV. CONCLUSION

This paper presents a comprehensive process for designing, simulating, fabricating, and verifying a micro-binary DOE to generate an AB. In this process, the CGH method is used as a design tool, and the simulation results are obtained using the Fresnel impulse response propagator in Fourier optics. The laser writing path is generated using a decision tree algorithm in machine learning and then input into the DLL system to produce the DOE pattern. The pattern is then etched into a chemical solution and evaluated using an optical verification system to ensure accuracy.

The experimental results match the design and simulation, demonstrating the effectiveness of the calculation and manufacturing method. The DOE pattern is compact, durable, and ready for use in any optical system without the need for additional support equipment. The design method is simple and contained within the software to ensure accuracy without the need for expensive additional software. The calculation process can be easily optimized for other methods or machine systems. Additionally, the DLL system does not require a mask and can be maintained in a standard room, making fabrication and maintenance costs reasonable. The chemical solution used for etching is safe, inexpensive, readily available, and can be used for an extended period of time under standard room conditions. These advantages make it possible to design and manufacture binary DOEs in various shapes and on micro- or even nano-scale dimensions with controllable parameters.

The shape of the AB can be easily controlled, including the dimensions of the pattern, the thickness of the curves, or its curvature, by adjusting the parameters in the design equation. Applications of the AB generated by the micro-binary DOE pattern are widespread and include optical trapping, micro-machining, and microscopy, giving it wide potential, not only academically but also industrially.

FUNDING

This work was supported in part by the Technology Innovation Program (Grant no. RS-2023-00237714, Development of Dynamic Metrology Tool for CMP Process Stabilization) funded By the Ministry of Trade, Industry & Energy (MOTIE, Korea) (Grant no. 1415187786) and in part by the Technology Innovation Program (20020311, Optical Technology for the Automatic Analysis of EUV Mask) funded by the Ministry of Trade, Industry & Energy (MOTIE, Korea).

ACKNOWLEDGMENTS

All authors contributed to the conception and design of the study. Material preparation, data collection, and analysis were performed by H. T. D. Trung, Y.-S. Ghim, and H.-G. Rhee. The first draft of the manuscript was written by H. T. D. Trung and all authors commented on previous versions of the manuscript. All authors read and approved the final manuscript.

DISCLOSURES

H. T. D. Trung, Y.-S. Ghim, and H.-G. Rhee declare that they have no conflicts of interest or financial conflicts to disclose.

DATA AVAILABILITY

The data that support the findings of this study are available from the corresponding author upon reasonable request.

REFERENCES

1. S. Feng, Z. Wang, X. Cheng, and X. Dun, “Design of diffractive optical element for ultra-thin deep ultraviolet imaging system,” Proc. SPIE **11617**, 116172A (2020).
2. C. Chang and A. Sakdinawat, “Ultra-high aspect ratio high-resolution nanofabrication for hard X-ray diffractive optics,” Nat. Commun. **5**, 4243 (2014).
3. J. Soltau, P. Meyer, R. Hartmann, L. Strüder, H. Soltau, and T. Salditt, “Full-field x-ray fluorescence imaging using a Fresnel zone plate coded aperture,” Optica **10**, 127–133 (2023).
4. H. H. Barrett and F. A. Horrigan, “Fresnel zone plate imaging of gamma rays; Theory,” Appl. Opt. **12**, 2686–2702 (1973).
5. N. Jiménez, V. R. García, L. M. G. Raffi, F. Camarena, and K. Staliunas, “Sharp acoustic vortex focusing by Fresnel-spiral zone plates,” Appl. Phys. Lett. **112**, 204101 (2018).
6. L. Zhang, H. Zhang, H. Huang, J. Wang, H. Zhou, and T. Yu, “Generation of ultra-intense vortex laser from a binary phase square spiral zone plate,” Opt. Express **32**, 5161–5173 (2024).
7. Y. Li, M. Guo, G. Guo, and Q. Ma, “Transdermal drug delivery mediated by acoustic vortex beam,” Ultrasonics **140**, 107304 (2024).

8. A. Sakdinawat and Y. Liu, "Soft-x-ray microscopy using spiral zone plates," Opt. Lett. **32**, 2635–2637 (2007).
9. S. N. Khonina, N. L. Kazanskiy, P. A. Khorin, and M. A. Butt, "Modern types of axicons: New functions and applications," Sensors **21**, 6690 (2021).
10. A. Vijayakumar and S. Bhattacharya, "Phase-shifted Fresnel axicon," Opt. Lett. **37**, 1980–1982 (2012).
11. G. Liang, S. Sun, J. Wang, Z. Qu, T. Wei, X. Liu, H. Sun, P. P. Monka, and A. Hamza, "Application of array Bessel beam generated by superposition method in electronic glass cutting," Opt. Lasers Eng. **181**, 108384 (2024).
12. T. Meinert and A. Rohrbach, "Light-sheet microscopy with length-adaptive Bessel beams," Biomed. Opt. Express **10**, 670–681 (2019).
13. A. Benstiti, A. Bencheikh, K. Ferria, S. Chabou, O. C. Boumeddine, "Generation of Flexible hyperbolic Airy-like beams using a truncated acousto optical effect," Opt. Commun. **505**, 127501 (2022).
14. F. Wang, D. Liu, and L. Wang, "Propagation of Airy beams in uniformly accelerated space," Opt. Commun. **537**, 129445 (2023).
15. Z. Liu, Z. Cui, L. Liu, X. Cao, and F. Wu, "Propagation properties of partially coherent Airy beams through the gradient-index medium," Appl. Opt. **63**, 6721–6729 (2024).
16. H. Moradi, M. Jabbarpour, D. Abdollahpour, and F. Hajizadeh, "3D optical trapping by a tightly focused circular airy beam," Opt. Lett. **47**, 4115–4118 (2022).
17. Z. Zheng, B.-F. Zhang, H. Chen, J. Ding, and H.-T. Wang, "Optical trapping with focused Airy beams," Appl. Opt. **50**, 43–49 (2011).
18. D. G. Papazoglou, N. K. Efremidis, D. N. Christodoulides, and S. Tzortzakis, "Observation of abruptly autofocusing waves," Opt. Lett. **36**, 1842–1844 (2011).
19. N. K. Efremidis and D. N. Christodoulides, "Abruptly autofocusing waves," Opt. Lett. **35**, 4045–4047 (2010).
20. T. Vettenburg, H. Dalgarno, J. Nylk, C. Coll-Lladó, D. E. K. Ferrier, T. Čižmár, F. J. Gunn-Moore, and K. Dholakia, "Light-sheet microscopy using an Airy beam," Nat. Methods **11**, 541–544 (2014).
21. J. Nylk, K. McCluskey, M. A. Preciado, M. Mazilu, Z. Yang, F. J. Gunn-Moore, S. Aggarwal, J. A. Tello, D. E. K. Ferrier, and K. Dholakia, "Light-sheet microscopy with attenuation-compensated propagation-invariant beams," Sci. Adv. **4**, eaar4817 (2018).
22. J. N. Cederquist and J. R. Fienup, "Analytic design of optimum holographic optical elements," J. Opt. Soc. Am. A **4**, 699–705 (1987).
23. M. R. Feldman and C. C. Guest, "Computer generated holographic optical elements for optical interconnection of very large scale integrated circuits," Appl. Opt. **26**, 4377–4384 (1987).
24. N. H. A. Nguyen, H.-G. Rhee, P. Kang, and Y.-S. Ghim, "Design and fabrication of an off-axis elliptical zone plate in visible Light," Curr. Opt. Photon. **6**, 44–50 (2022).
25. C. Han, Y. Tang, X. Cheng, H. Sun, J. Feng, and S. Hu, "A novel coaxial focus position detection technique based on differential modulation evaluation for laser direct photolithography," Opt. Lasers Eng. **161**, 107396 (2023).
26. N. H. A. Nguyen, H.-G. Rhee, Y.-S. Ghim, "Design and lithographic fabrication of elliptical zone plate array with high fill factor," Curr. Opt. Photon. **5**, 8–15 (2021).
27. T. D. T. Hieu, N. V. H. Linh, A. Munnibee, Y. J. Kim, Y. S. Ghim, and H. G. Rhee, "Design and fabrication of a Fresnel zone plate with an enhanced depth of focus," Appl. Opt. **63**, 6384–6392 (2024).
28. N. H. A. Nguyen, H. Rhee, and Y. S. Ghim, "Novel fabrication and designs for hybrid optical elements with wider angle field of view by using integrated direct laser lithographic system," Opt. Lasers Eng. **170**, 107774 (2023).
29. Z. X. Fang, Y. X. Ren, L. Gong, P. Vaveliuk, Y. Chen, and R. D. Lu, "Shaping symmetric Airy beam through binary amplitude modulation for ultralong needle focus," J. Appl. Phys. **118**, 203102 (2015).
30. R. Dharmavarapu, A. Vijayakumar, and S. Bhattacharya, "Design and fabrication of holographic optical elements for the generation of tilted and accelerating Airy beams," Asian J. Phys. **24**, 1363–1372 (2015).
31. G. A. Siviloglou and D. N. Christodoulides, "Accelerating finite energy Airy beams," Opt. Lett. **32**, 979–981 (2007).
32. M. V. Berry and N. L. Balazs, "Nonspreading wave packets," Am. J. Phys. **47**, 264–267 (1979).
33. G. A. Siviloglou, J. Broky, A. Dogariu, and D. N. Christodoulides, "Observation of accelerating Airy beams," Phys. Rev. Lett. **99**, 213901 (2007).
34. A. Vijayakumar and S. Bhattacharya, *Design and Fabrication of Diffractive Optical Elements with MATLAB* (SPIE Press, USA, 2017), Chapter 7.
35. D. Voelz, *Computational Fourier Optics: A MATLAB Tutorial* (SPIE Press, USA, 2011), p. 52, 64, 65, 66.
36. E. Wolf and E. W. Marchand, "Comparison of the Kirchhoff and the Rayleigh–Sommerfeld theories of diffraction at an aperture," J. Opt. Soc. Am. **54**, 587–594 (1964).
37. T. Liu, Q. Liu, S. Yang, Z. Jiang, T. Wang, and G. Zhang, "Investigation of axial and transverse focal spot sizes of Fresnel zone plates," Appl. Opt. **56**, 3725–3729 (2017).
38. S. Xue, Q. Liu, T. Liu, S. Yang, P. Su, K. Liu, B. Tian, and T. Wang, "Electromagnetic exploration of focusing properties of high-numerical-aperture micro-Fresnel zone plates," Opt. Commun. **426**, 41–45 (2018).